

# A hard x-ray split-and-delay unit for the HED Instrument at the European XFEL

Sebastian Roling<sup>1\*</sup>, Victor Kärcher<sup>1</sup>, Liubov Samoylova<sup>2</sup>, Karen Appel<sup>2</sup>, Stefan Braun<sup>3</sup>, Peter Gawlitza<sup>3</sup>, Frank Siewert<sup>4</sup>, Ulf Zastra<sup>2</sup>, Matthias Rollnik<sup>1</sup>, Frank Wahlert<sup>1</sup>, and Helmut Zacharias<sup>1\*</sup>

<sup>1</sup>Physikalisches Institut, WWU Münster, Wilhelm-Klemm Straße 10, 48149 Münster, Germany

<sup>2</sup>European XFEL GmbH, Holzkoppel 4, 22869 Schenefeld, Germany

<sup>3</sup>Fraunhofer Institut IWS, Winterbergstraße 28, 01277 Dresden, Germany

<sup>4</sup>Helmholtz-Zentrum für Materialien und Energie, Albert-Einstein-Straße 15, 12489 Berlin, Germany

\*corresponding authors: s\_rol02@uni-muenster.de, h.zacharias@uni-muenster.de

## ABSTRACT

For the High Energy Density Instrument (HED) at the European XFEL a hard x-ray split-and-delay unit (SDU) is built covering photon energies in the range between 5 keV and 24 keV. This SDU enables time-resolved x-ray pump / x-ray probe experiments as well as sequential diffractive imaging on a femtosecond to picosecond time scale. The set-up is based on wavefront splitting that has successfully been implemented at an autocorrelator at FLASH. The x-ray FEL pulses will be split by a sharp edge of a silicon mirror coated with Mo/B<sub>4</sub>C and W/B<sub>4</sub>C multilayers. Both partial beams then pass variable delay lines. For different photon energies the angle of incidence onto the multilayer mirrors is adjusted in order to match the Bragg condition. Hence, maximum delays between +/- 1 ps at 24 keV and up to +/- 23 ps at 5 keV will be possible. Time-dependent wave-optics simulations are performed with Synchrotron Radiation Workshop (SRW) software. The XFEL radiation is simulated using the output of the time-dependent SASE code FAST. For the simulations diffraction on the edge of the beam-splitter as well as height and slope errors of all eight mirror surfaces are taken into account. The impact of these effects on the ability to focus the beam by means of compound refractive lenses (CRL) is analyzed.

## 1. INTRODUCTION

In this paper a novel x-ray split-and-delay unit based on wavefront beam splitting and multilayer mirror coatings is described. It covers photon energies between  $h\nu = 5$  keV and  $h\nu = 24$  keV. With this spectral range the SDU will enable jitter-free hard x-ray pump/ hard x-ray probe experiments at the High Energy Density Instrument (HED) [1] at the SASE 2 undulator of the European XFEL [2]. In the hard x-ray regime single coatings at grazing angles larger than  $\theta = 0.2^\circ$  show a high absorbance and a small reflectivity. Thus, multilayer mirrors are utilized in order to facilitate sufficiently large incident angles corresponding to maximum possible delays in the picosecond range. The x-ray pulses are split at a sharp edge of a wavefront beam-splitter and then propagate through two delay branches with adjustable optical path lengths. For the XUV and soft x-ray spectral regime a similar set-up with carbon coatings instead of multilayer mirrors has been integrated into the FLASH SASE FEL [3]. With this device the spatio-temporal coherence properties [4,5] as well as the pulse duration [6] of a soft x-ray FEL have successfully been measured for the first time. Further, ionization dynamics in expanding clusters [7] and in iodine molecules [8] have been investigated by XUV pump / XUV probe spectroscopy, the ultrafast heating of hydrogen has been studied [9,10], and femtosecond sequential imaging has been realized for the first time [11]. The new SDU at the HED Instrument at the European XFEL will enable similar experiments in the hard x-ray spectral regime.

In order to evaluate the influence of the device on experiments with focused hard x-ray pulses, time-dependent wave-optics simulations have been performed by means of Synchrotron Radiation Workshop (SRW) software for SASE

pulses at  $h\nu = 5$  keV. This software tool has recently been applied to assess the capability of the SDU to measure the temporal coherence properties of hard x-ray FEL-pulses [12]. For this earlier study, diffraction at the beam splitter and a one-dimensional cut through the surface profile was taken into account. At the HED instrument, the XFEL radiation will be focused by means of compound refractive lenses (CRL) in order to perform experiments with intense, focused hard x-ray pulses. The results of these experiments severely depend on the fluence and the spatial shape of the beam that is obtained in the focal area. Therefore, in this paper the impact of wave-front distortions on the spatial intensity profile in the focus is analyzed. For this purpose, the entire optical layout of the SDU, including diffraction on the beam splitter edge and the two-dimensional surface profiles of all eight mirrors are taken into account.

## 2. OPTICAL CONCEPT

The optical concept of an SDU has to meet various requirements, like: a high reflectivity, transmission of the whole spatial beam profile, transmission of the spectral bandwidth of the XFEL pulse (0.08% - 0.2%, which corresponds to  $\Delta E \sim 6.4$  to 16 eV at  $h\nu = 8$  keV), a delay with sub-fs resolution, a large delay range, and the wide photon energy range of the XFEL (5 – 24 keV). These properties have to be achieved with a minimal disturbance of the beam position and direction, a high mechanical stability making a temporal resolution in the sub-100 attosecond regime feasible. The design incorporates elements, which allow a realization of the SDU in a practicable size of  $L = 6$  m.

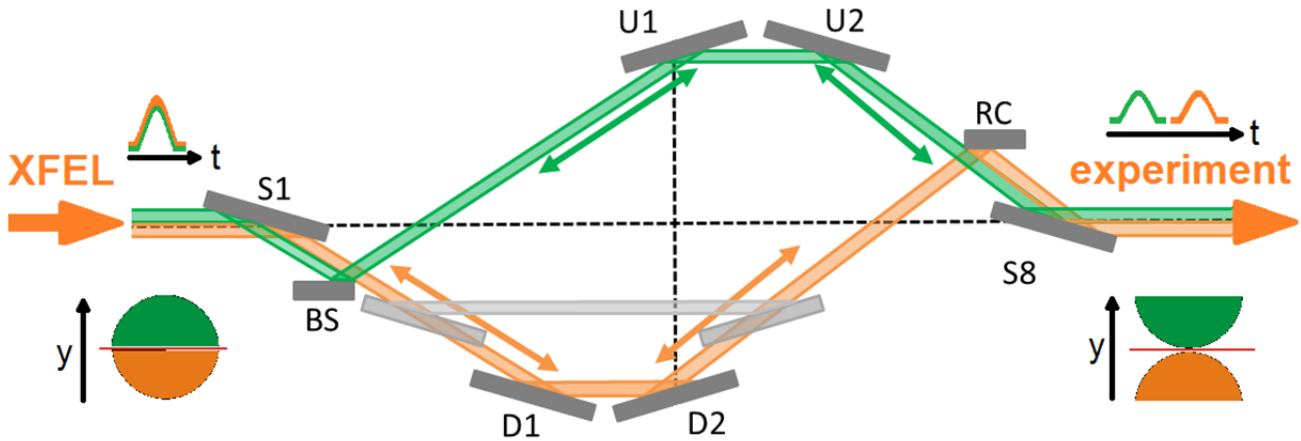


Fig.1: Schematic drawing of the optical layout of the x-ray split- and delay-unit.

In order to meet these requirements a point symmetric optical concept based on a geometrical wavefront beam splitter and multilayer Bragg coatings which permit larger grazing angles is applied. The set-up of the optical pathway is schematically shown in Fig. 1. The XFEL beam enters the SDU from the left side and is reflected by the first mirror (S1) downwards in the direction of the beam splitter (BS). The lower green part of the beam is reflected into the upper delay arm while the upper orange part passes the sharp edge in the direction of the lower delay arm. The mirrors of both delay arms can be moved along the split beam direction in order to introduce a temporal delay between both partial beams. After the orange beam has passed over the lower delay line it is reflected by the recombination mirror (RC) in the direction of the last mirror (S8). The green beam passes the sharp edge of the recombination mirror unaffected. Thus, in this point symmetric concept the recombination mirror acts as the counterpart of the beam-splitter. The last mirror (S8) reflects both beams into their original direction. It should be noted that the beam shape of both arms is rotated by  $180^\circ$  due to the odd number of reflections. In order to perform experiments the beams have to be overlapped. This can be achieved by slightly rotating the recombination mirror, RC.

As already mentioned the multilayer mirrors are intended to work at Bragg angles depending on the photon energy. Therefore, for different photon energies not only the angles of the mirrors but the whole beam path has to be adjusted.

### 3. MECHANICAL LAYOUT

The projected sub-fs resolution as well as the essential pointing stability of the partial beams demand for a substantial mechanical stability of the 6 m long construction. A picture of the SDU during the construction phase is shown in figure 2. An intrinsic mechanical stabilization of the entire system is achieved by increasing the stiffness of the whole system. Thereby vibrations are significantly reduced. To ensure the mechanical sturdiness all components are mounted inside an optical bench which consists of an octagonal structure made out of stainless steel. The FEL beam is divided geometrically and both partial beams travel along two paths whose lengths can be adjusted. The pathlength difference of one beam with respect to the other and in consequence the temporal delay is changed by moving the mirrors of both arms along guide rails. These rails are supported by stainless steel frames. The mirrors are mounted to girders that are moved along the guide rails by means of recirculating ball drives.

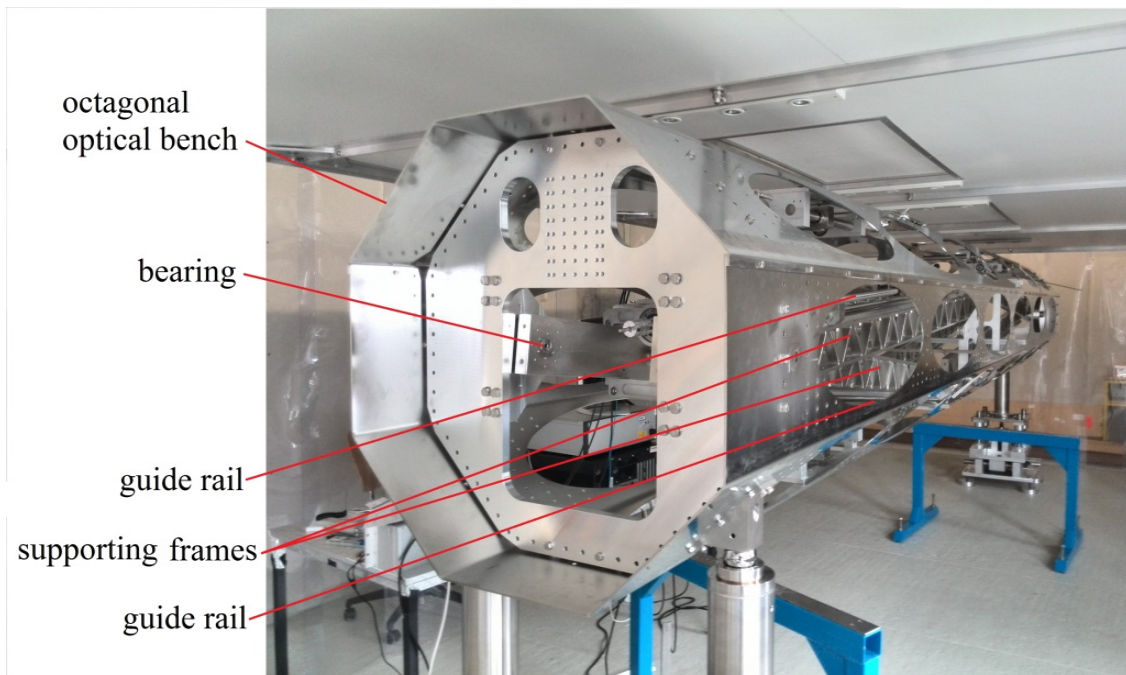


Figure 2: The SDU during the construction phase.

Since the grazing angles of multilayer mirrors depend on the photon energy, an adjustability of the angle of incidence is required. In order to adjust the correct angles for different photon energies all mirrors are turnable and the angle of the guide rails is variable. The mirror mountings possess stepper motor drives with an angular precision of better than  $\Delta\alpha = 1 \mu\text{rad}$ .

By moving the mirror the path length which the beam travels along the hypotenuse instead of the (shorter) adjacent of a triangle is varied, compare Fig. 1. To obtain the designed sub-100 attosecond resolution of the delay this longitudinal motion of the mirrors has to be very precise. At a grazing angle of  $\theta = 0.57^\circ$  (for  $h\nu = 20 \text{ keV}$ ) a movement of the mirror of  $\Delta l = 10 \mu\text{m}$  results in a pathlength difference of the light of 1.9 nm which corresponds to a temporal delay of  $\Delta t = 6 \text{ as}$ . If the grazing angle is  $\theta = 1.83^\circ$  (for  $h\nu = 5 \text{ keV}$ ) the corresponding delay for a movement of  $\Delta l = 10 \mu\text{m}$  is  $\Delta t = 100 \text{ as}$ .

When the delay is changed by moving the mirrors an angular error of the mirrors on the order of  $\Delta\theta = 5 \mu\text{rad}$  occurs due to the interaction of the bearing balls with the guides rails. This error is compensated by means of an active tracking system. To achieve this the angle of the mirror at the current position is measured by a three-axis interferometer and corrected by a piezo actuator. In order to provide the experiments with an unaffected XFEL beam the whole optical bench can be moved horizontally so that the beam does not hit any mirror of the SDU.

## 4. MIRRORS

### 4.1 Multilayer coating

For photon energies between  $5 \text{ keV} < h\nu < 10 \text{ keV}$  Ni/B<sub>4</sub>C coatings with a period of  $d = 4 \text{ nm}$  are applied on all mirrors except for BS and RC. These two mirrors reflect the beam at Bragg angles twice as large compared to the other mirrors as it is obvious from Fig.1. Here W/B<sub>4</sub>C coatings with a period of  $d = 1.96 \text{ nm}$  are applied since Ni/B<sub>4</sub>C coatings with a period below  $d = 3 \text{ nm}$  cannot be manufactured due to interdiffusion processes between the layers. For photon energies above  $h\nu = 10 \text{ keV}$  Mo/B<sub>4</sub>C multilayers with a period of  $d = 3.2 \text{ nm}$  are used. Since the Bragg angle varies as a function of the photon energy also the maximum possible delay will vary between  $\Delta t_{\text{max}} = 23 \text{ ps}$  at  $h\nu = 5 \text{ keV}$  and  $\Delta t_{\text{max}} = 1.0 \text{ ps}$  at  $h\nu = 24 \text{ keV}$ , see table 1.

It is possible to choose between different mirror coatings by moving the whole set-up horizontally. For two-color experiments with fundamental and third harmonic radiation a third coating has been applied on the mirrors S1 and S8 because these two mirrors will have to reflect both photon energies at the same Bragg angle.

Table 1: The total transmission and the maximum delay times

Photon energy [keV]	Angle BS/RC [°]	Multilayer Material	Angle S1/S8, U1/U2, D1/D2 [°]	Multilayer Material	Delay [ps]	Transmission
5	3.690	W/B <sub>4</sub> C	1.846	Ni/B <sub>4</sub> C	23	0.23-0.33
6	3.070	W/B <sub>4</sub> C	1.538	Ni/B <sub>4</sub> C	16	0.33-0.43
8	2.305	W/B <sub>4</sub> C	1.153	Ni/B <sub>4</sub> C	9	0.47-0.57
10	1.841	W/B <sub>4</sub> C	0.923	Ni/B <sub>4</sub> C	6	0.14-0.18
12	1.535	W/B <sub>4</sub> C	0.768	Ni/B <sub>4</sub> C	4	0.16-0.22
8	2.849	Mo/B <sub>4</sub> C	1.425	Mo/B <sub>4</sub> C	14	0.10-0.22
10	2.278	Mo/B <sub>4</sub> C	1.142	Mo/B <sub>4</sub> C	9	0.16-0.30
12	1.900	Mo/B <sub>4</sub> C	0.949	Mo/B <sub>4</sub> C	6	0.21-0.38
15	1.591	Mo/B <sub>4</sub> C	0.758	Mo/B <sub>4</sub> C	4	0.27-0.45
18	1.266	Mo/B <sub>4</sub> C	0.631	Mo/B <sub>4</sub> C	3	0.29-0.50
20	1.138	Mo/B <sub>4</sub> C	0.567	Mo/B <sub>4</sub> C	2.3	0.14-0.29
20	0.928	W/B <sub>4</sub> C	0.464	Ni/B <sub>4</sub> C	1.5	0.48-0.57
24	0.770	W/B <sub>4</sub> C	0.385	Ni/B <sub>4</sub> C	1.0	0.57-0.66

Since this is not possible with a single coating, a novel two-color multilayer Bragg mirror has been developed [14]. This mirror consists of a Si substrate that is coated with two different types of multilayer systems,  $n = 120$  Mo/B<sub>4</sub>C layers with a periodicity of  $d = 3.2 \text{ nm}$  directly on the substrate and  $n = 4$  Ni/B<sub>4</sub>C layers with a periodicity of  $d = 11.85 \text{ nm}$  on top. Fundamental radiation with photon energies between  $3 \text{ keV}$  and  $9 \text{ keV}$  is reflected by a Ni/B<sub>4</sub>C multilayer system while the third harmonic ( $9 \text{ keV} < h\nu < 20 \text{ keV}$ ) passes this system and is reflected by the Mo/B<sub>4</sub>C multilayers. The reflectance of this novel two-color hard x-ray multilayer Bragg mirror has experimentally been evaluated at the ESRF. The reflectance amounts to  $R = 0.73$  and  $R = 0.78$  for the fundamental photon energies at  $h\nu = 5 \text{ keV}$  and  $h\nu = 6 \text{ keV}$ , respectively. For the corresponding third harmonic radiation reflectances of  $R = 0.70$  and  $R = 0.75$  at  $h\nu = 15 \text{ keV}$  and  $h\nu = 18 \text{ keV}$  were determined.

### 4.2 Mirror substrates

For the simulations the knowledge of the mirror profiles is required in order to evaluate the impact of figure deviations on the wave front of the XFEL pulse. For this purpose the mirrors were inspected by use of the Nanometer Optic component measuring Machine (NOM) [15] at the BESSY-II metrology laboratory at HZB in Berlin. The NOM allows a precise measurement of such optics by use of slope measuring deflectometry with sub-nm precision [16] and a spatial

resolution of 1.7 mm up to a length of 1200 mm [17]. Figure 3 exemplarily shows the surface profile of the beam splitter (BS).

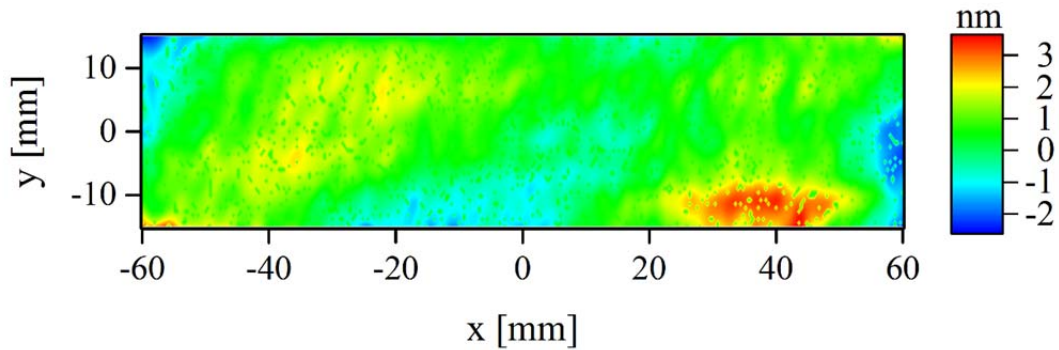


Figure 3: The height profile of the mirror used for the wavefront propagation simulation.

The  $l = 120$  mm long mirror shows height deviations between  $h = -2.4$  nm and  $h = 3.2$  nm resulting in a maximum peak-to-valley error of  $\Delta h = 5.6$  nm.

### 4.3 Wavefront propagation

The SRW software based on a Fourier optics approach and Wavefront Propagation (WPG) framework provides a powerful tool for the simulation of the wavefront propagation of XFEL pulses [18, 19]. It offers a comprehensive and extendable toolbox that is capable of solving a wide range of XFEL optics problems. The software takes into account the optics imperfections and allows modelling essential optical elements such as grazing incidence plane and focussing mirrors and gratings. The optical performance of the SDU mirrors was evaluated by means of a Python script that incorporates the SRW and WPG library.

The wavefront propagation simulations were carried out for a photon energy of  $h\nu = 5$  keV. SASE pulses with a pulse energy of  $E_{\text{pulse}} = 1$  mJ and a coherence time that amounts to  $t_c = 0.243$  fs were generated by the three-dimensional SASE code FAST [19]. The angular divergence of the pulses was  $\Theta = 3.87$   $\mu\text{rad}$ . After leaving the undulator the beam propagates towards the SDU which is located at  $z = 846$  m behind the undulator. For the simulations, the two-dimensional surface profile of all eight mirrors is taken into account. Behind the SDU the two partial beams propagate and irradiate the detector in the experimental area at  $z = 972$  m.

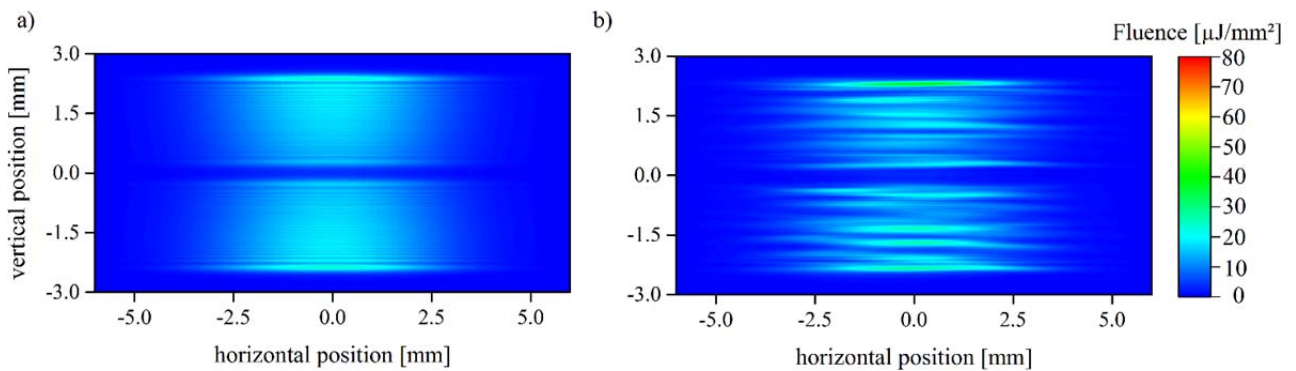


Figure 4: The two separated, unfocused partial beams on the detector for a photon energy of  $h\nu = 5$  keV with perfect mirrors in the SDU (a) and for the mirrors used in the SDU (b).

Figure 4 shows the separated unfocused two partial beams on the detector for a photon energy of  $h\nu = 5$  keV with perfect mirrors in the SDU (a) and for mirrors with the surface errors that were evaluated by means of the NOM (b). In

figure 4(a) only fringes from diffraction at BS and RC are visible. In figure 4(b) also fringes caused by wavefront distortions that are induced by the non-perfect mirror surfaces occur. The maximum fluence in the irradiated area amounts to  $F = 36 \mu\text{J}/\text{mm}^2$  for ideal mirrors and  $F = 49 \mu\text{J}/\text{mm}^2$  for real mirror surfaces.

When both partial beams are overlapped by slightly rotating the recombination mirror (RC) interference fringes appear for zero delay as it is obvious from Fig. 5(a) and 5(b) for ideal mirrors and for non-perfect mirror surfaces, respectively. The maximum fluence here amounts to  $F = 69 \mu\text{J}/\text{mm}^2$  and  $F = 81 \mu\text{J}/\text{mm}^2$ , respectively.

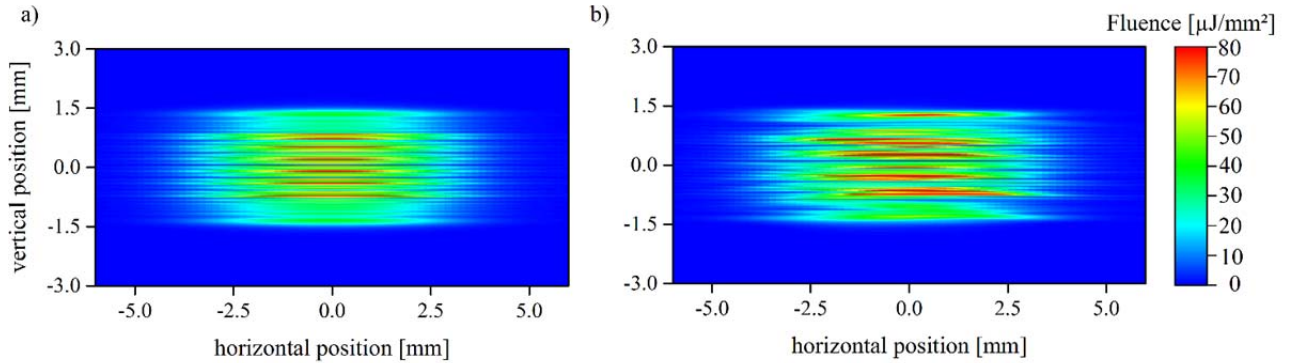


Figure 5: The two overlapped, unfocused partial beams on the detector for a photon energy of  $h\nu = 5 \text{ keV}$  with perfect mirrors in the SDU (a) and for the mirrors used in the SDU (b).

In order to focus the x-ray pulses into the experimental area at  $z = 972 \text{ m}$  parabolic CRL lenses can be moved into the beam at  $z = 229 \text{ m}$  and at  $z = 962 \text{ m}$  [1]. Figure 6 shows the focused XFEL beam without the SDU. A beam diameter of  $d = 22 \mu\text{m}$  (FWHM) results and the maximum fluence amounts to  $F = 0.11 \text{ J}/\text{mm}^2$ .

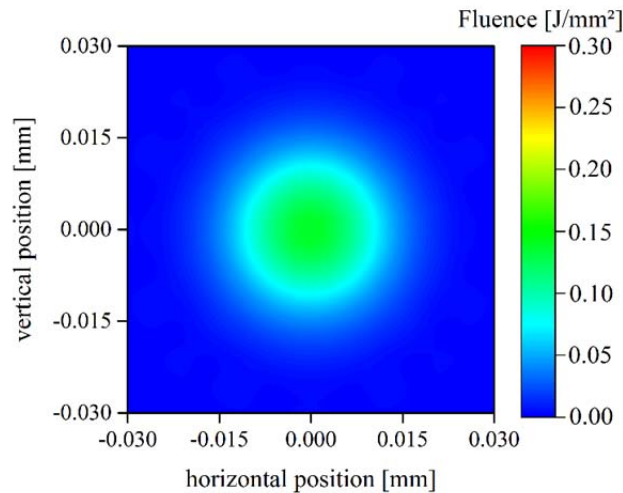


Figure 6: Simulated focused XFEL beam at  $z = 972 \text{ m}$  with a beam diameter of  $d = 22 \mu\text{m}$  (FWHM).

When the SDU is moved into the beam, the XFEL pulses are split and fringes caused by the edge of the beam splitter occur as it can be seen in Fig. 7(a) for ideal mirror surfaces. The maximum fluence amounts to  $F = 0.12 \text{ J}/\text{mm}^2$ . With additional modulations that are caused by non-ideal mirrors the maximum fluence increases to  $F = 0.15 \text{ J}/\text{mm}^2$ , compare Fig. 7(b).

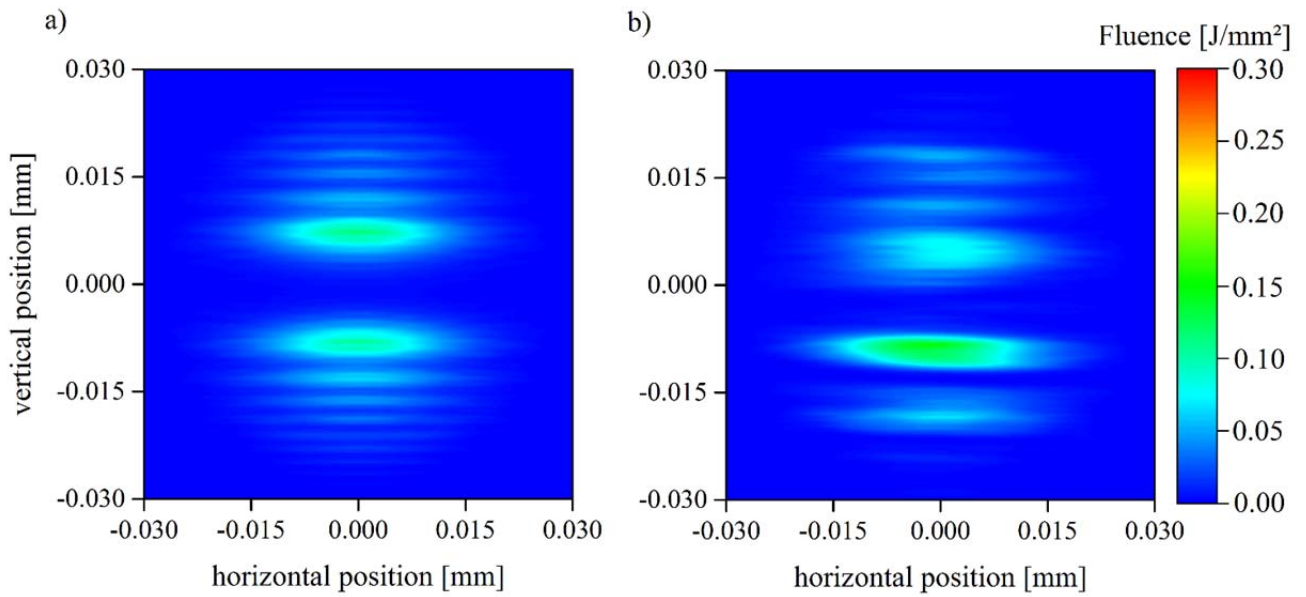


Figure 7: The intensity profiles of separated partial beams in focal plane for ideal (a) and non-ideal (b) mirror surfaces.

The corresponding situation for overlapping partial beams is depicted in Fig. 8(a) and (b) for ideal and non-ideal mirror surfaces, respectively. Due to the additional time-dependent interference fringes at zero delay the maximum amounts to  $F = 0.25 \text{ J/mm}^2$  and  $F = 0.31 \text{ J/mm}^2$  for ideal and non-ideal mirror surfaces, respectively.

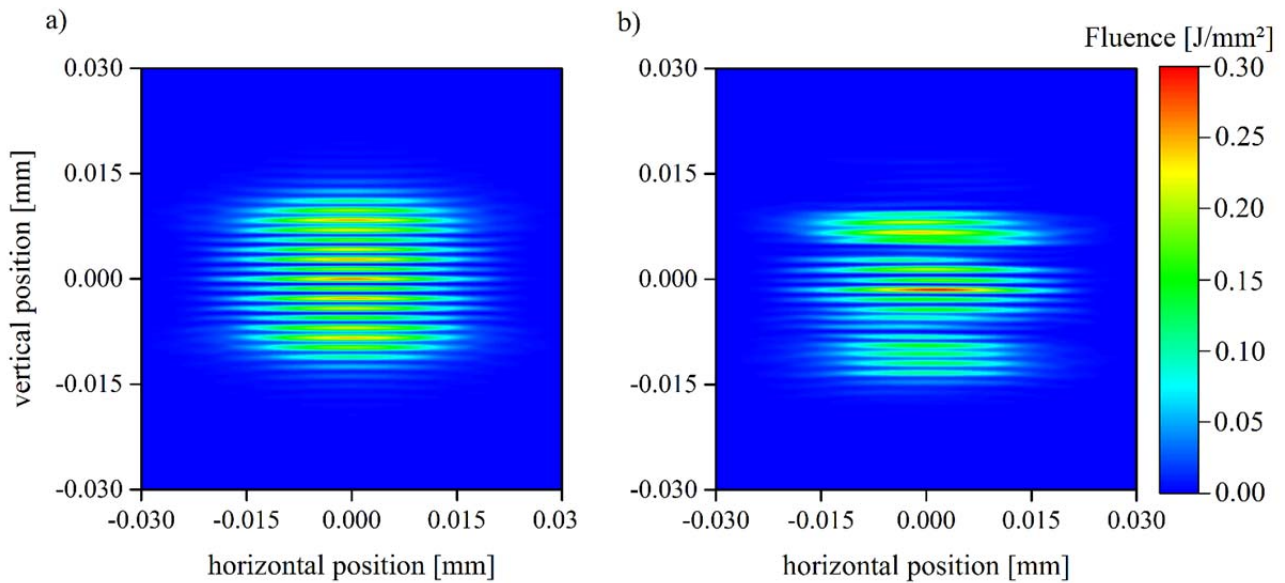


Figure 8: The intensity profiles of overlapped partial beams in focal plane for ideal (a) and non-ideal (b) mirror surfaces.

## 5. CONCLUSION

A new split- and delay-unit for the European XFEL is built for photon energies between  $h\nu = 5$  keV and 24 keV. This SDU will serve the users with two time-delayed x-ray pulses for x-ray pump / x-ray probe experiments and it will enable a characterization of the temporal properties of the XFEL. Multilayer coated mirrors are used in order to provide sufficiently steep angles to enable maximum delays between  $\Delta t = 1.0$  ps at  $h\nu = 24$  keV and  $\Delta t = 23$  ps at  $h\nu = 5$  keV. The impact of optics imperfections on the spatial intensity properties of focused XFEL pulses is evaluated by means of wavefront propagation simulations that are performed with SRW and WPG framework.

## ACKNOWLEDGEMENT

This work is supported by the BMBF (project: 05K10PM2, 05K13PM1 and 05K16PM2).

## REFERENCES

- [1] M. Nakatsumi et al., Scientific Instrument High Energy Density Physics (HED), XFEL.EU TR-2014-001 (2014)
- [2] M. Altarelli et al., The European X-Ray Free Electron Laser Technical Design Report, DESY Hamburg (2006)
- [3] M. Wöstmann et al., J. Phys. B: At. Mol. Opt. Phys. **46**, 164005 (2013)
- [4] R. Mitzner et al., Opt. Expr. **16**, 19909-19919 (2008)
- [5] S. Roling et al., Phys. Rev. ST Accel. Beams **14**, 080701 (2011)
- [6] R. Mitzner et al., Phys. Rev. A **80**, 025402 (2009)
- [7] M. Krikunova et al., J. Phys. B: At. Mol. Opt. Phys. **45**, 105101 (2012)
- [8] K. Schnorr et al., Phys. Rev. Lett. **113**, 073001 (2014)
- [9] U. Zastra et al., Phys. Rev. Lett. **112**, 105002 (2014)
- [10] U. Zastra et al., Phys. Rev. E **90**, 013104 (2014)
- [11] C.M. Günther et al., Nat. Phot **5**, 99-102 (2011).
- [12] S. Roling et al., Phys. Rev. STAB **17**, 110705 (2014)
- [13] A. Snigirev et al., Nature **384**, 49 (1996)
- [14] S. Roling et al., Opt. Lett. **39**, 2782 (2014)
- [15] F. Siewert et al., Nucl. Instr. Meth. in Phys. Res. A **635**, 52 (2011)
- [16] F. Siewert et al., Opt. Expr. **20**, 4526 (2012)
- [17] F. Siewert et al., Nucl. Instr. Meth. in Phys. Res. A **710**, 422 (2013)
- [18] O. Chubar et al., Nucl. Instr. Meth. in Phys. Res. A **593**, 30 (2008)
- [19] A. Buzmakov et al., Proc. SPIE 9209, 9209-32 (2014)
- [19] E. Saldin et al., Nucl. Instr. Meth. in Phys. Res. A **429**, 233 (1999)